10

Spectral properties of composite materials based on nanoporous high-silica glasses activated by silver and lanthanum ions

© M.A. Girsova, G.F. Golovina, I.N. Anfimova, L.N. Kurilenko, A.S. Saratovskii

Grebenschikov Institute of Silicate Chemistry RAS, 199034 Saint-Petersburg, Russia

e-mail: girsovama@yandex.ru

Received June 09, 2023
Revised October 27, 2023
Accepted October 29, 2023

Spectral properties of composite materials based on matrices of high-silica porous glasses activated by silver ions and lanthanum ions have been investigated. The optical density spectra (270−900 nm) and infrared transmittance spectra (11000−9000 and 9000−4000 cm^{-1}) of composite materials of different compositions subjected to heat treatment according to one of three modes (120, 500 and 800°C) have been considered. The synthesized composite materials were investigated by X-ray powder diffraction method and energy-dispersive X-ray spectroscopy. The analysis of optical spectra permitted to identify the formation of molecular clusters, clusters, dimers and silver nanoparticles, as well as absorption bands related to charge transfer $O^{2+} \rightarrow La^{3+}$ (282, 285, 300 nm) and to lanthanum nanoparticles (282, 285 nm) under different conditions of synthesis of composite materials. It was found that the change in the mode of thermal treatment of composites leads to changes in the IR spectra of composites, and the change in their composition leads to the appearance of additional bands associated with the oxygen atom of the OH-group, which can coordinate with several neighboring lanthanum atoms.

Keywords: composite materials, high-silica porous glass, silver, lanthanum, near infrared spectroscopy, optical spectroscopy, X-ray powder diffraction method, energy-dispersive X-ray spectroscopy.

DOI: 10.61011/EOS.2023.10.57762.5304-23

Introduction

Materials activated by silver in the presence of/without lanthanum can be applied as nanocatalysts and in sensor applications as well (gas sensors, colorimetric sensors), in nanophotonics, for solar cells, for optical devices, optical memory [1–5]. The ion La^{3+} has an unfilled orbital ($4f^0 5d^0 6s^0$), thereby it is quite stable and captured holes can be easily released [6]. This mechanisms can be described by the following equations (1)–(4) (see the equations (3), (5)−(7)) of the work [6]):

$$O^{2-} + h^+ \rightarrow O^-, \quad (1)$$

$$La^{3+} + O^- \rightarrow La^{4+} + O^{2-} \quad (2)$$

„hole trap“,

$$La^{4+} + OH^- \rightarrow La^{3+} + OH \quad (3)$$

„hole release“,

$$2Ag^0 + O_2 \rightarrow 2Ag^+ + O^{2-} \quad (4)$$

„electron release“.

It is known that La_2O_3 has a wide band gap (4.3 eV) [7,8], while the edge of fundamental absorption is within the region below 250 nm [9]. The work [8] has shown the influence of an annealing temperature (from 400 to 800°C) on a structure and optical properties of the films La_2O_3, and on their semiconductor properties as well (the band gap increases from 4.17 to 5.11 eV with increase in the annealing temperature). Our previous works [10–12] have shown that thermal treatment of the composite materials (CMs), containing ions, nanoparticles (NPs), molecular clusters (MCs) of silver, in the presence/without ions of cerium or erbium affects the concentration distribution of the elements along the thickness of the CM samples (energy-dispersive X-ray spectroscopy), the structure (IR spectroscopy within the frequency region from 1100−400 cm^{-1}) and the spectral properties of the CMs (optical spectroscopy). The work [13] has noted that thermal treatment (annealing) of the materials, simultaneously activated by silver and lanthanum, leads to the formation of the nanoparticles of La_2O_3 and silver, which favourably affects the spectral-luminescent properties of the materials (the photoluminescence intensity increases).

An important task of the present work is to select temperature-time modes of CM synthesis in order to effectively control the formation of the oxides of silver and lanthanum, the nanoparticles and the molecular clusters of silver in nanoscale structures, avoiding clusterization effects. It has included investigation of the influence of the chemical composition and the mode of CM thermal treatment on their spectral properties in UV, visible and near IR ranges of the spectrum.

Objects and methods of investigation

The investigated objects are the composite materials based on high-silica porous glasses (PG-8V-NT-120) activated by the silver ions in the presence or without the

lanthanum ions, which have been synthesized by single-stage impregnation.

The PG-8V-NT-120 samples (the average pore diameter within the range 3−5 nm, the porosity ∼ 30%) of the thickness of 1.5 ± 0.15 mm were produced as per the procedure [14]. Analytical chemistry methods was taken to determine the composition of the PG matrices (PG-8V-NT-120) by the analysis (mas%): 0.30 Na_2O, 3.14 B_2O_3, 0.11 Al_2O_3, 96.45 SiO_2, as specified in [14]. The samples of the PG matrices were impregnated in the aqueous salt solutions $AgNO_3$ with adding or without $La(NO_3)_3$ (the weight ration of nitrates in the Ag/La solution was 1:1 and 10:1), with subsequent thermal treatment of the composite materials in air atmosphere as per the specially developed temperature-time modes with isothermal holding at the temperature of $T_{h.t.} = 120$, 500 and 800°C in according to a procedure used in [15]. It is known that thermolysis of lanthanum nitrate at 780−800°C results in formation of lanthanum oxide La_2O_3 [15,16]. At the temperature above 300°C, silver nitrate is decomposed to produce Ag^0 [16], while in according to data of the work [17] the thermolysis of $AgNO_3$ occurs at 360−515°C. It should be taken into account that La_2O_3 is crystallized in the air atmosphere at 800°C as per [7]. The synthesized samples 100Ag, 100Ag/10La, 100Ag/100La have been designated in accordance with the concentration of impregnation solutions. The solutions for the CM synthesis were prepared using such reagents as silver nitrate $AgNO_3$ (reagent grade, chemically pure, 99.9%), 6-aqueous lanthanum nitrate $La(NO_3)_3 \cdot 6H_2O$ (reagent grade, chemically pure, 99.0%). In the composite materials 100Ag, 100Ag/10La, 100Ag/100La, the content of silver and alkali metals was determined using flame photometry on the spectrophotometer iCE 3000 (Thermo Fisher Scientific). It was (mas%) (0.14−0.20) Na_2O, (0.01−0.05) K_2O, (0.60−0.79) Ag_2O. The standard square deviation for Na_2O was 0.2−1.1%, so was for K_2O — 0.1−0.5%, so was for Ag_2O — 0.1−0.8%. Previously, the IR spectroscopy (1000−400 cm^{-1}) of [15] has been used to investigate series of the samples 100Ag ad 100Ag/100La at 120, 500 and 800°C. It found the bands corresponding to the presence of Ag_2O, La_2O_3 and to vibrations of the bands Ag−O, Ag−O−Ag, O−Ag−O, La−O−H and La−O. Using the energy-dispersive X-ray spectroscopy, it was found that the content of silver in CM 100Ag/100La (at 500°C) changes along the thickness of the CM samples within 1.15−4.45 mas% (the average value of 3.40 ± 0.26 mas%), and lanthanum is distributed quite evenly within 0.71−1.15 mas% (the average value of 0.85 ± 0.18 mas%) except for the surface layer (∼ 40−65 nm) [15].

The composite materials 100Ag, 100Ag/10La, 100Ag/100La as compared to PG-8V-NT-120 were investigated using the near IR spectroscopy (Fig. 1−4) at the room temperature by means of the spectrophotometer FSM-2211 within the frequency region of 11000−9000 and 9000−4000 cm^{-1}, with spectrum resolution of 2 cm^{-1}. When operating in the spectrum range of 11000−9000 cm^{-1}, a receiver is to be the Si photodiode, so is within the range of 9000−4000 cm^{-1} — the InGaAs photodiode. A radiation source is to be a halogen lamp. The composite materials 100Ag, 100Ag/10La, 100Ag/100La were investigated within the range of 270−900 nm (Fig. 5) using the spectrophotometer SF-2000. With the least spectral resolvable interval of 1 nm, the limit of allowable value of absolute error of the unit was ±0.4 nm for the spectrum range of 270−390 nm, so was ±0.8 nm for 390−900 nm. When operating in the spectrum range of 190−390 nm, the radiation source was a deuterium lamp, so was a halogen lamp within the range of 390−1100 nm. The spectra of transmittance and optical density were measured at the room temperature on the samples of the composite materials and PG-8V-NT-120 made as plane-parallel plates of the thickness of 1.50 ± 0.15 mm. X-ray powder diffraction method of the CM powders was carried out using the diffractometer Rigaku Ultima IV (Japan). Copper anode radiation of $\lambda(CuK_\alpha) = 1.5418$ Åwas used. The X-ray diffraction patterns were taken in the angle range 2θ from 5 to 80°. The scanning rate by 2θ was 3°/min. The ICDD PDF-2 (2022) diffraction database was used to interpretation the diffraction reflexes. The elemental composition of the composites was studied using the energy-dispersive X-ray spectroscopy (EDX). The linear profiles of elemental concentration were measured with an increment of 35−47 μm. The measurements were taken on the scanning election microscope CamScan MX2500 equipped with the energy-dispersive spectrometer Link Pentafet (Oxford Instruments, Si(Li)-detector with the area of 10 mm^2 and the resolving power of 138 eV (for Mn-K_α-radiation)). The CM samples were pressed into polymeric washers, polished, and carbon was sputtered to the surface. The measurements were performed at the plane-parallel plates of the thickness of 1.50 ± 0.15 mm.

Investigation results

Fig. 1−3 shows the IR spectra of transmittance (within the frequency range of 11000−9000 and 9000−4000 cm^{-1}) for the composites of the composition of 100Ag, 100Ag/10La, 100Ag/100La, which have been produced by thermal treatment at 120, 500 and 800°C.

Fig. 4, *a* shows the IR spectra of transmittance for PG-8V-NT-120 within the frequency ranges of 11000−9000 and 9000−4000 cm^{-1}. Fig. 4, *a* clearly shows the absorption bands at 10732, 10458, 8113, and at 7317, 7133, 6876, 5272, 4548 cm^{-1} as well.

Table 1 specifies the absorption bands detected in CMs and PG-8V-NT-120 and the identification of the bands as well. All the composites (regardless of the composition and the mode of thermal treatment) and the PG-8V-NT-120 have detected four groups of the bands: at 10762−10730, 7335−7317, 5284−5267 and 4554−4523 cm^{-1}. It has established the influence of CM thermal treatment resulting in appearance/disappearance of the bands. The

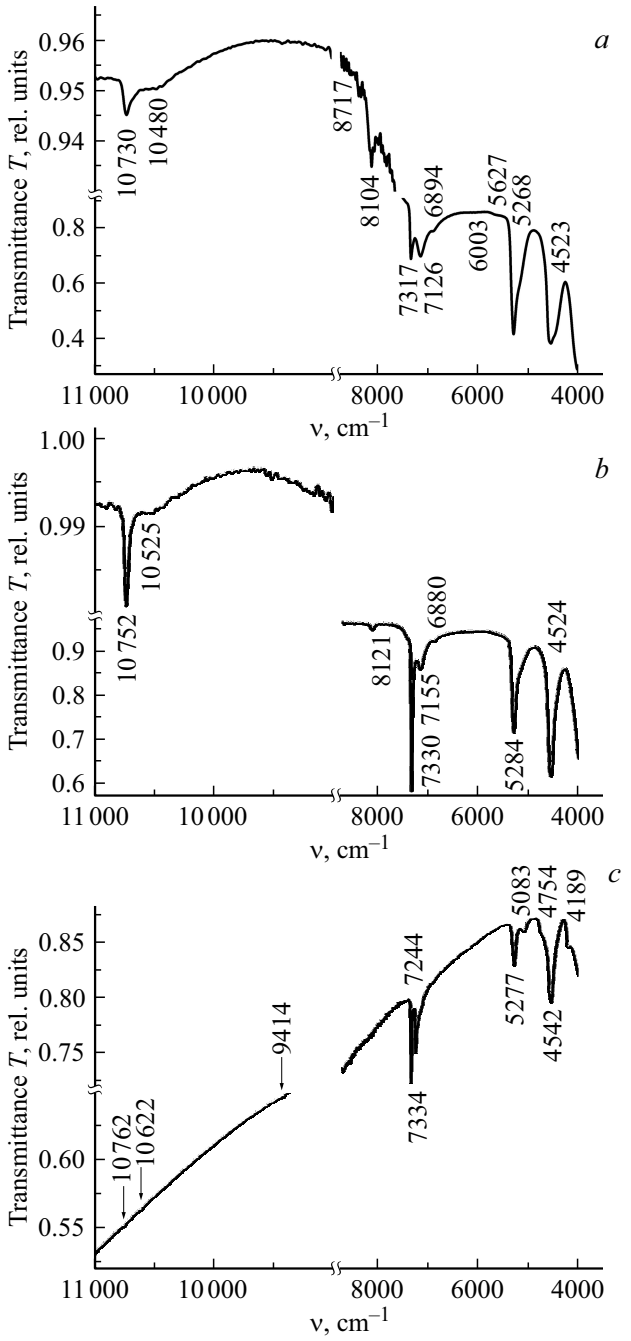

Figure 1. Transmittance spectra of the composite material 100Ag depending on the temperature of thermal treatment: *a* — 120°C, *b* — 500°C, *c* — 800°C.

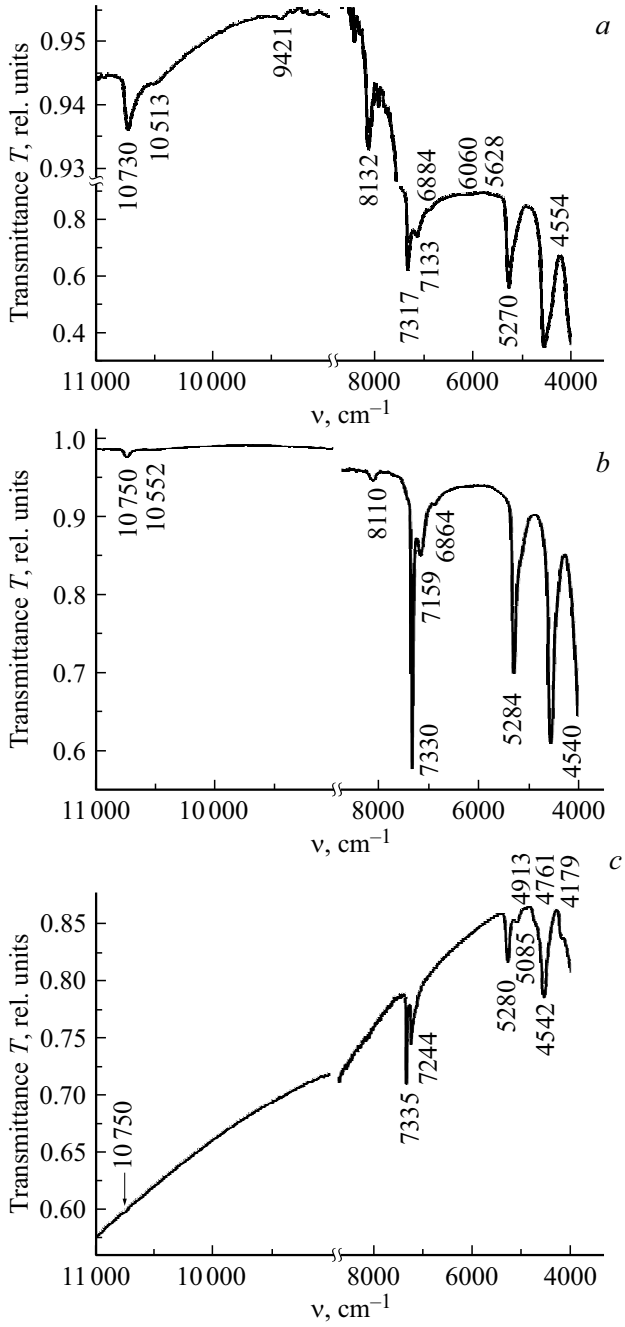

Figure 2. Transmittance spectra of the composite material 100Ag/10La depending on the temperature of thermal treatment: *a* — 120°C, *b* — 500°C, *c* — 800°C.

composite materials (regardless of the composition), dried at 120°C, are characterized by additional bands in six frequency regions: at 10513–10480, 8132–8104, 7133–7126, 6894–6870, 6060–6003, 5662–5627 cm^{-1}. Besides, CMs 100Ag and 100Ag/10La (at 120°C) have detected another additional band each at 8717 and 9421 cm^{-1}, thereby indicating the influence of the CM chemical composition. With the increase in the temperature of CM thermal treatment (at 500°C), the additional bands within the four frequency regions (at 10585–10504, 8123–8110, 7159–7155, 6880–6864 cm^{-1}) remain at all the composite materials (regardless of the composition), while the bands at 6060–6003 and 5662–5627 cm^{-1} disappear. The composite material 100Ag/100La (at 500°C) has been found two more bands: at 9295 and 9108 cm^{-1}, thereby indirectly indicating the influence of the chemical composition of the composite material. The composite materials thermally treated at 800°C there's a disappearance of the bands in several frequency regions, but the additional bands have

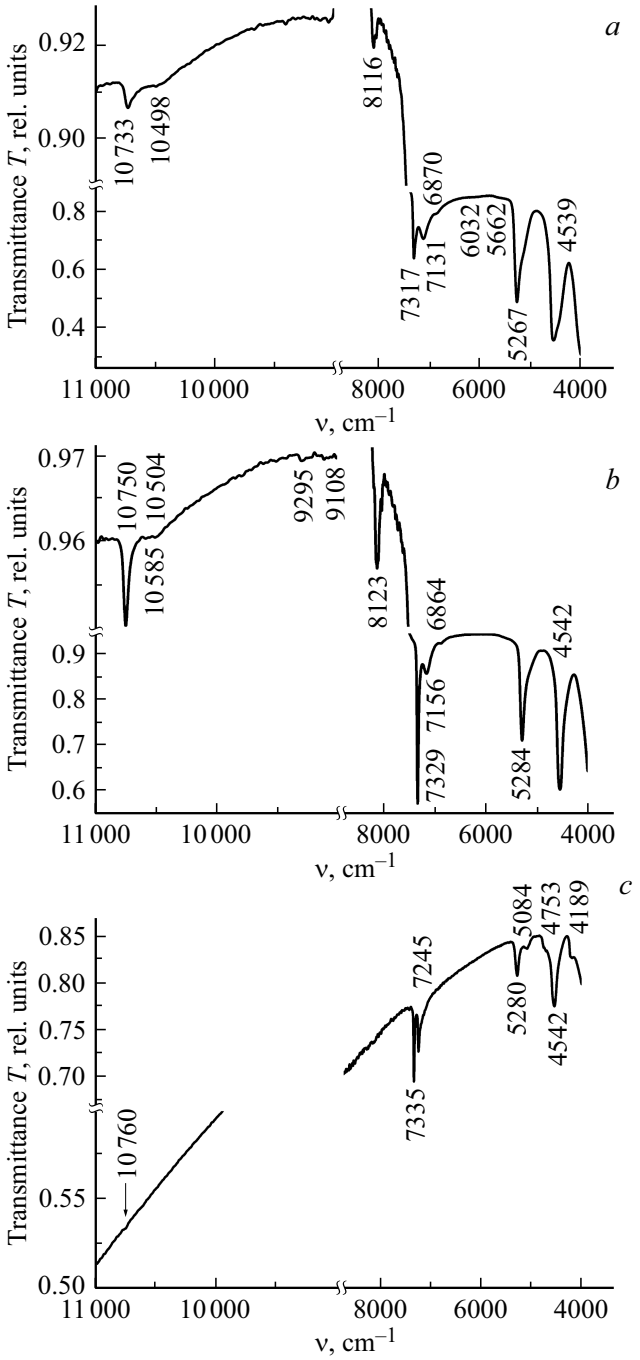

Figure 3. Transmittance spectra of the composite material 100Ag/100La depending on the temperature of thermal treatment: *a* — 120°C, *b* — 500°C, *c* — 800°C.

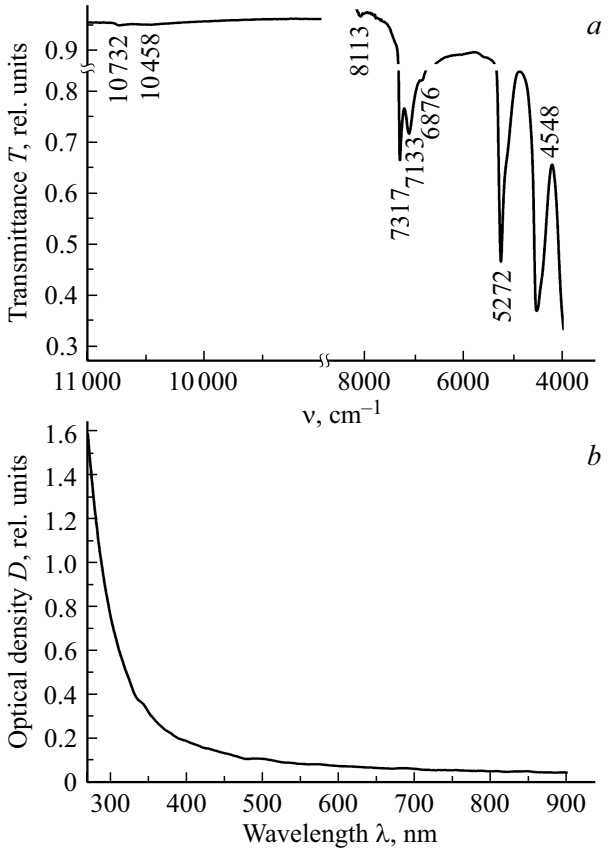

Figure 4. Spectra of transmittance (*a*) and optical density (*b*) for PG-8V-NT-120.

been found at all the composite materials, too (regardless of the composition): at 7245–7244, 5085–5083, 4761–4753, 4189–4179 cm^{-1}. The influence of the composition of the composite material has also been established. For the composite material 100Ag (at 800°C), two additional bands have been detected at 10622 and 9414 cm^{-1}, so has for the composite material 100Ag/10La (at 800°C) — at 4913 cm^{-1}.

It has established the substantial influence of the mode of CM thermal treatment (120, 500 and 800°C), which exhibits in appearance/disappearance of the additional bands. It is known that the following processes are typical when heating the porous glasses (see review in [18–22]). When $T_{h.t.} \leq 200$°C, the physically adsorbed water is removed. Within the temperature region of 200–600°C, the coordinatively-bound water is removed. At the temperatures of 600–800°C, the bound silanol groups are dehydroxylated and softening of the silica framework. Further increase in the temperature is accompanied by irreversible dehydroxylation and condensation of the silanol groups at the surface of the adjacent walls of pores, thereby resulting in pore closure.

The influence of the chemical composition of the composite material shows up only in appearance of the additional bands at 10622, 9421, 9414, 9295, 9108, 8717, 4913 cm^{-1}, which are typical for the individual composite materials. It is known that $La(NO_3)_3 \cdot 6H_2O$ and La_2O_3 are hygroscopic substances, which increase the OH vibrations and increase amount of water [23]. It is possible that the additional bands appear at 9421, 9295, 9108, 4913 cm^{-1} due to possible coordination of the atom of oxygen of the OH group to the several adjacent atoms of lanthanum [23,24].

It should be noted that at 800°C, all the CM series demonstrate the decrease in the intensity of the absorption

Table 1. Absorption bands (within the range of $11000-4000\,cm^{-1}$) detected at CMs depending on the composition and the temperature of thermal treatment, as compared to PG-8V-NT-120

Designation of the glasses and the composites, temperature of CM thermal treatment Position of the absorption bands, cm^{-1}										Assignment of the bands
PG-8V-	CM 100Ag			CM 100Ag/10La			CM 100Ag/100La			
NT-120	120°C	500°C	800°C	120°C	500°C	800°C	120°C	500°C	800°C	
10732	10730	10752	10762 10622	10730	10750	10750	10733	10750 10585	10760	$3\nu(OH_{free})$, ν(Si-OH), $3\nu_3$OH
10458	10480	10525		10513	10552		10498	10504		
			9414	9421				9295 9108		$2\nu_3(OH) + 2\nu_1(SiO_4)$, the oxygen atom of the OH-group can coordinate to several adjacent atoms of lanthanum
	8717									$2\nu_3(OH) + 2\nu_1(SiO_4)$
8113	8104	8121		8132	8110		8116	8123		$2\nu(OH_{free}) + \nu$(Si-O), $2\nu_3(OH) + \nu_1(SiO_4)$
7317	7317	7330	7334	7317	7330	7335	7317	7329	7335	$2\nu_3(OH)$, ν(Si-OH)
			7244			7244			7245	$\nu(B^{III}-OH)$, $2\nu_3(OH)$
7133	7126	7155		7133	7159		7131	7156		absorption of the hydroxyl groups and the water molecules adsorbed on the surface
6876	6894	6880		6884	6864		6870	6864		absorption of the capillary-condensed water molecules
	6003			6060			6032			$\nu_{sym}(OH)$
	5627			5628			5662			$(\delta + \nu)(H_2O)$
5272	5268	5284	5277	5270	5284	5280	5267	5284	5280	absorption of the hydroxyl groups and surface-absorbed molecules of water, $(\delta + \nu)(H_2O)$
			5083			5085			5084	absorption of the water molecules coordinatively bound to the impurity atoms of boron
						4913				$(\delta + \nu)$(OH), $\nu(B^{III}-OH)$, the oxygen atom of the OH-group can coordinate to several adjacent atoms of lanthanum
			4754			4761			4753	ν(OH), $\nu(B^{IV}-OH)$
4548	4523	4542	4542	4554	4540	4542	4539	4542	4542	δ(Si−OH), ν(OH), ν(Na−OH), $(\delta + \nu)$(Si−OH)
			4189			4179			4189	ν(OH) with a low lattice vibration frequency

bands within the entire frequency range, while transmittance within the frequency range of $11000-9000\,cm^{-1}$ as compared to CM (at 120 and 500°C) significantly decreases. It can indirectly indicate decrease in the number of the OH groups and amount of water in CMs with increase in the temperature of thermal treatment.

The observed weak bands at $10762-10730\,cm^{-1}$ ($\sim 929-932$ nm), $10622-10458\,cm^{-1}$ ($\sim 941-956$ nm) can be assigned to the second overtone of stretching vibrations of the free OH groups ($3\nu(OH_{free})$), to the second overtone of stretching vibrations of the Si−OH-groups ν(Si−OH) and to vibrations of the OH groups ($3\nu_3(OH)$) [25–27]. The additional bands of the weak intensity at $9421-9414\,cm^{-1}$ ($\sim 1061-1062$ nm), $9295\,cm^{-1}$ (~ 1076 nm), $9108\,cm^{-1}$ (~ 1098 nm) can be related to a combination of the stretching vibrations $2\nu_3(OH) + 2\nu_1(SiO_4)$ [26].

Now, let us consider the frequency region of $9000-4000\,cm^{-1}$. The additional weak absorption band at $8717\,cm^{-1}$ (~ 1147 nm) observed at CM 100Ag only, can be related to the combination of the stretching vibrations $2\nu_3(OH) + 2\nu_1(SiO_4)$ [26]. The bands at $8132-8104\,cm^{-1}$ ($\sim 1230-1234$ nm), which can be detected at PG-8V-NT-120 and at all the CMs (regardless of the composition) at 120 and 500°C, are, most likely, assigned to the combination of the first overtone of the stretching vibrations of the free OH groups on the surface of the porous glass and of the stretching vibrations of

the Si−O-bonds $2\nu(OH_{free}) + \nu(Si-O)$ [25], and can be related to the combination of the stretching vibrations $2\nu_3(OH) + \nu_1(SiO_4)$ [26]. It is possible that the bands at 7335−7317 cm^{-1} (∼ 1363−1367 nm) found at all the CMs and PG-8V-NT-120, are probably related to the first overtone of the stretching vibrations of the $2\nu_3$ OH groups and the ν Si−OH groups [10,25–27,28–30]. Thermal treatment of CMs at 800°C results in appearance of the additional absorption bands at 7245 and 7244 cm^{-1} (∼ 1380 nm), which can be assigned to the vibrations of the ν B^{III}−OH groups, where boron is in the trigonal coordination [28–31], and to the overtone of the stretching vibrations of the $2\nu_3$ OH groups [26].

PG-8V-NT-120 and all the CMs (regardless of the composition) at 120 and 500°C were found to have the bands at 7159−7126 cm^{-1} (∼ 1397−1403 nm) and the weak bands at 6894−6864 cm^{-1} (∼ 1451−1457 nm). The first group of the bands is, most likely, assigned to absorption of the hydroxyl groups and the surface-adsorbed molecules of water, so are the second weak bands — to absorption of the capillary-condensed molecules of water [10,25,28–31]. The additional bands of low intensity observed the CMs at 120°C at 6060−6003 cm^{-1} (∼ 1650−1666 nm) and 5662−5627 cm^{-1} (∼ 1766−1777 nm) can be attributed to the overtone of the symmetrical stretching vibrations of the OH groups $\nu_{sym}(OH)$ and to the combination of bending and stretching vibrations of water $(\delta + \nu)(H_2O$, respectively [30,32].

PG-8V-NT-120 and all the CMs were detected the bands at 5284−5267 cm^{-1} (∼ 1893−1899 nm) and at 4554−4523 cm^{-1} (∼ 2196−2211 nm). The first group of the bands can be assigned to absorption of the hydroxyl groups and the surface-adsorbed molecules of water, to the combination of bending and stretching vibrations of water $((\delta + \nu)(H_2O))$, so can the second group of the bands — to the bending vibrations of the Si−OH-groups $(\delta(Si-OH))$, to the stretching vibrations of the OH groups $(\nu(OH))$ and the Na−OH groups $(\nu(Na-OH))$, to the combination of the bending and stretching vibrations of the Si−OH groups $((\delta + \nu)(Si-OH))$, respectively [10,28–31]. Thermal treatment of CMs at 800°C (regardless of the composition) results in appearance of the additional absorption bands in the three frequency regions: 5085−5083 cm^{-1} (∼ 1967 nm), 4761−4753 cm^{-1} (∼ 2100−2104 nm), 4189−4179 cm^{-1} (∼ 2387−2393 nm), and to the absorption band of weak intensity at CM 100Ag/10La at 4913 cm^{-1} (2035 nm) as well. The bands at 5085−5083 cm^{-1} can be attributed to absorption of water molecules, coordinatively bound to the impurity atoms of boron [29–31]. The bands at 4761−4753 cm^{-1} are, most likely, related to the stretching vibrations of the OH groups $(\nu(OH))$ and the B^{IV}−OH groups $(\nu(B^{IV}-OH))$, where boron is in the tetrahedral coordination [33]. The bands at 4189−4179 cm^{-1} can be related to the stretching vibrations of the OH groups $(\nu(OH))$ with the low lattice vibration frequency [29–31,34]. The weak band at 4913 cm^{-1} can be attributed to the combination of the bending and stretching vibrations of the OH groups $((\delta + \nu)(OH))$, to the stretching vibrations of the B^{III}−OH groups $(\nu(B^{III}-OH))$, where boron is in the trigonal coordination [33,34].

Previously, it had been established that the PG-8V-NT-120 matrices were characterized by the edge of fundamental absorption at 240 nm [28]. Fig. 4, *b* shows the optical density spectrum of PG-8V-NT-120 within the range of 270−900 nm. No absorption band has been observed in the specified range, but an edge of the strong UV band is visible.

Fig. 5 shows the CM optical density spectra depending on the composition (100Ag, 100Ag/10La, 100Ag/100La) and the mode of CM thermal treatment (120, 500 and 800°C) within the range of 270−900 nm. Table 2 summarizes all the data on the detected CM absorption bands and their deciphering as per the literature data (see review in [11], [35–53]).

The spectral dependencies of optical density for CMs 100Ag, dried at 120°C, show weak absorption bands at 400 nm (∼ 3.10 eV), 473 nm (∼ 2.62 eV), 739 nm (∼ 1.68 eV). With introduction of lanthanum, CMs 100Ag/10La, dried at 120°C, exhibit additional bands at 489 nm (∼ 2.54 eV) and 570 nm (∼ 2.18 eV), and the band at 742 nm (∼ 1.67 eV) as well, and for CMs 100Ag/100La at 120°C the bands are detected only at 397 nm (∼ 3.12 eV) and 740 nm (∼ 1.68 eV). It is evident that the CM composition absorption influences a shape of the spectra, the intensity and the position of the absorption bands, and result in appearance of the additional absorption bands as well (489, 570 nm).

Thermal treatment of CMs at 500°C results in further change of the shape of the spectra, which appear as an increase in the optical density intensity within the spectrum's UV region. For CM 100Ag, it has been established that it had an additional UV absorption band of strong intensity at 315 nm (∼ 3.94 eV) and the band remained at 734 nm (∼ 1.69 eV). The CM 100Ag/10La is characterized by an additional UV absorption band of strong intensity at 300 nm (∼ 4.13 eV), too, and a band at 747 nm (∼ 1.66 eV). With increase in the lanthanum concentration, an additional band of weak intensity appears on the spectrum of CM 100Ag/100La at 535 nm (∼ 2.32 eV), so does a band at 745 nm (∼ 1.66 eV). It indicates that the CM composition and the mode of thermal treatment effect on the appearance of the additional absorption bands as compared to the dried CM samples.

Further increase in the temperature of CM thermal treatment (at 800°C) results in abrupt increase in the optical density intensity within the entire range (270−900 nm), which is manifested, inter alia, by the increase in the intensity of the absorption bands and the number thereof as compared to the CMs thermally treated at 120 and 500°C. The same nature of the spectra appear as for all the CM series. Besides, thermal treatment of the CM series 100Ag/10La and 100Ag/100La at 800°C results in substantial changes in the shape of the spectra as

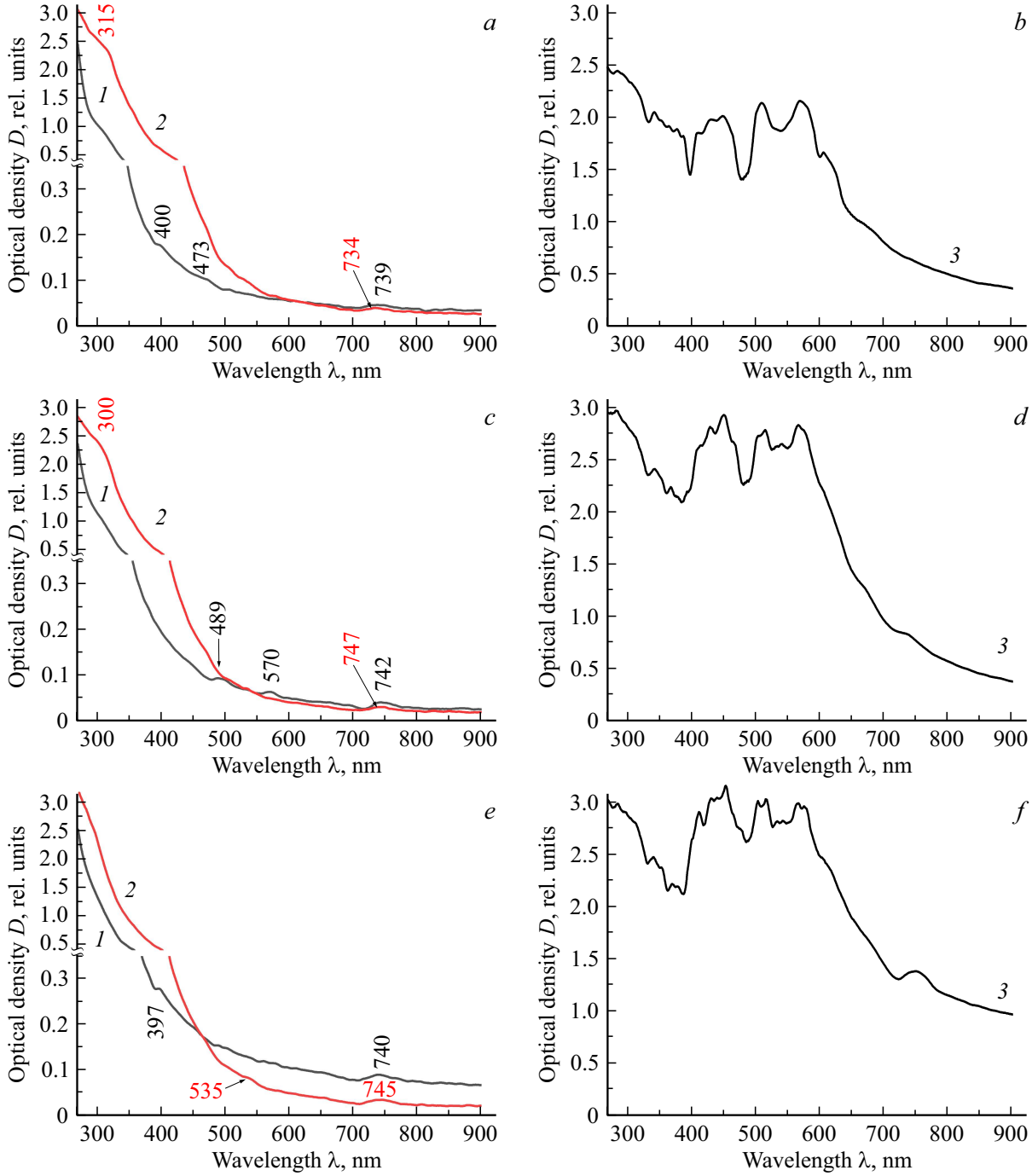

Figure 5. CM optical density spectra depending on the composition (*a, b* — 100Ag, *c, d* — 100Ag/10La, *e, f* — 100Ag/100La) and the temperatures of thermal treatment: *1* — 120°C, *2* — 500°C, *3* — 800°C.

compared to CM 100Ag at the same mode of treatment.

For CM 100Ag (at 800°C), the bands are found, with the maxima at 286 nm (~ 4.34 eV), 343 nm (~ 3.62 eV), 388 nm (~ 3.20 eV), 412 nm (~ 3.01 eV), 431 nm (~ 2.88 eV), 449 nm (~ 2.76 eV), 510 nm (~ 2.43 eV), 569 nm (~ 2.18 eV), 606 nm (~ 2.05 eV), 664 nm (~ 1.87 eV). For CM 100Ag/10La (800°C), the bands are showing, with the maxima at 282 nm (~ 4.40 eV), 343 nm (~ 3.62 eV), 368 nm (~ 3.37 eV), 414 nm (~ 3.00 eV), 429 nm (~ 2.89 eV), 451 nm (~ 2.75 eV), 465 nm (~ 2.67 eV), 504 nm (~ 2.46 eV), 515 nm (~ 2.41 eV), 541 nm (~ 2.29 eV), 566 nm (~ 2.19 eV), 670 nm (~ 1.85 eV), 735 nm (~ 1.69 eV).

For CM 100Ag/100La (800°C), the bands are visible, with the maxima at 285 nm (~ 4.35 eV), 341 nm (~ 3.64 eV), 353 nm (~ 3.51 eV), 370 nm (~ 3.35 eV), 376 nm (~ 3.30 eV), 411 nm (~ 3.02 eV), 430 nm

Table 2. Absorption bands (within the range of 270–900 nm) detected at CM depending on the composition and the temperature of thermal treatment

Designation of the glasses and the composites, temperature of CM thermal treatment. Position of the absorption bands, nm									Assignment of the bands
CM 100Ag			CM 100Ag/10La			CM 100Ag/100La			
120°C	500°C	800°C	120°C	500°C	800°C	120°C	500°C	800°C	
		286			282			285	MCs Ag_4, clusters Ag_4^{2+} and Ag_8^{2+}, due to charge transfer $O^2 \rightarrow La^{3+}$, Lanthanum NPs
				300					MCs Ag_1, MCs Ag_4, MCs Ag_9, neutral atoms Ag^0, due to charge transfer $O^2 \rightarrow La^{3+}$
	315								molecular ions Ag_2^+, MCs Ag_1
		343			343			341	neutral atoms Ag_0, MCs Ag_6 and Ag_7
								353	MCs Ag_3, La_2O_3
					368			370	MCs Ag_3, MCs Ag_5 and MCs Ag_5^+, La_2O_3
								376	MCs Ag_5, La_2O_3
		388							MCs Ag_2, Ag_3, Ag_4 and Ag_8
400						397			MCs Ag_4, Ag_6, clusters Ag_8^{2+}
		412			414			411	MCs Ag_2, silver NPs
		431			429			430	MCs Ag_4, silver NPs
		449			451			453	MCs Ag_3, silver NPs
473					465			475	dimers $Ag^+ - Ag^+$
			489						MCs Ag_3 and Ag_4
					504			503	MCs Ag_5, silver NPs
		510			515			515	MCs Ag_3, silver NPs
							535	533	MCs Ag_7, silver NPs, silver clusters, including Ag_m^{n+} ($m \geq 8$, $n \leq 4$)
					541			541	silver NPs, silver clusters, including Ag_m^{n+} ($m \geq 8$, $n \leq 4$)
		569	570		566			566	silver NPs, silver clusters, including Ag_m^{n+} ($m \geq 8$, $n \leq 4$)
								575	silver NPs, silver clusters, including Ag_m^{n+} ($m \geq 8$, $n \leq 4$)
		606						603	silver NPs, silver clusters, including Ag_m^{n+} ($m \geq 8$, $n \leq 4$)
		664			670				silver NPs, silver clusters, including Ag_m^{n+} ($m \geq 8$, $n \leq 4$)
739	734		742	747	735	740	745	748	silver NPs, silver clusters, including Ag_m^{n+} ($m \geq 8$, $n \leq 4$)

(~ 2.88 eV), 453 nm (~ 2.74 eV), 475 nm (~ 2.61 eV), 503 nm (~ 2.47 eV), 515 nm (~ 2.41 eV), 533 nm (~ 2.33 eV), 541 nm (~ 2.29 eV), 566 nm (~ 2.19 eV), 575 nm (~ 2.16 eV), 603 nm (~ 2.06 eV), 748 nm (~ 1.66 eV).

It should be noted that for all the CM series (100Ag, 100Ag/10La and 100Ag/100La) at 800°C the absorption bands are found, with the maxima at 282–286, 341–343, 411–414, 429–431, 449–453, 510–515, 566–569 nm. The additional bands at 388, 510, 606, 664 nm (CM 100Ag), at 368, 465, 504, 541, 670, 735 nm (CM 100Ag/10La) and at 353, 370, 376, 475, 503, 533, 541, 575, 603, 748 nm (CM 100Ag/100La) directly indicate the influence of the CM composition on the spectral properties.

Now, let us describe the absorption bands found within the range of 270–900 nm. The UV bands with the maxima at 282–286 nm, observed at CMs at 800°C, are, most likely, related to MCs Ag_4 and the clusters Ag_4^{2+} and Ag_8^{2+} [35–39]. Besides, the wide UV bands with the maxima at 282 and 285 nm can be assigned to charge transfer $O^{2-} \rightarrow La^{3+}$, and can be related to absorption of the lanthanum NPs. [40,41]. The additional UV absorption band at 300 nm, belonging to CM 100Ag/10La (at 500°C), can be due to formation of MCs Ag_1, MCs Ag_4, MCs Ag_9 and to the neutral atoms Ag^0 [35,42,43–45], and as well as due to charge transfer $O^{2-} \rightarrow La^{3+}$ [40]. For CM 100Ag (at 500°C), we observe the UV band at 315 nm, which can be attributed to the molecular ions Ag_2^+ and MCs Ag_1 [11,43,44,46]. The UV absorption bands at 341–343 nm, observed for CM at 800°C, can be related to the neutral atoms Ag^0 and MCs Ag_6 and Ag_7 [11,42,43,46]. The UV band at 353 nm can indicate formation of MCs Ag_3 [42,44], so can the UV bands at 368 and 370 nm — MCs Ag_3, MCs Ag_5 and MCs Ag_5^+ [36,43], and so can at 376 nm — to MCs Ag_5 [42]. The absorption bands at 353, 368, 370, 376 nm can be related to absorption of La_2O_3 [47]. The band at 388 nm is, most likely, caused by formation of MCs Ag_2, MCs Ag_3, MCs Ag_4 and MCs Ag_8 [42–45]. The absorption bands of weak intensity for CM 100Ag at 397 and 400 nm and for CM 100Ag/100La at 120°C can be related to MCs Ag_4, Ag_6 and to clusters Ag_8^{2+} [35–37,42]. The wide bands with the maxima at 411–414, 429–431, 449–453 nm are typical for the silver NPs with surface plasmonic resonance (SPR) (see review in [11]), [35,46,48–51]. Besides, the bands at 411–414 nm can indicate formation of MCs Ag_2 [43]. The bands at 429–431 nm can be attributed to MCs Ag_4 [43], so can the bands at 449–453 nm — to MCs Ag_3 [44]. The absorption band of weak intensity at 473 nm for CM 100Ag at 120°C is, most likely, assigned to the dimers $Ag^+–Ag^+$ [52], while the band shift towards longer wavelengths (at 489 nm) for CM 100Ag/100La at 120°C may be related to formation of MCs Ag_3 and Ag_4 [42–44]. The presence of the additional absorption bands at 465 and 475 nm for CM 100Ag/10La and CM 100Ag/100La at 800°C can occur due to the dimers $Ag^+–Ag^+$ [52]. The wide bands with the maxima at 503–504 and 515 nm for CM 100Ag/10La and CM 100Ag/100La at 800°C, and the band at 510 nm for CM 100Ag at 800°C can be related to the presence of MCs Ag_5 and MCs Ag_3 , respectively, [36,43], and to formation of the silver NPs with SPR [11,48]. The additional absorption bands at 535 and 533 nm observed at CMs 100Ag/100La at 500 and 800°C can be attributed to formation of the silver nanoparticles with SPR, to MCs Ag_7, and to various silver clusters, including Ag_m^{n+} ($m \geq 8$, $n \leq 4$) [11,43,48,53]. The band at 541 nm, detected at CMs 100Ag/10La and KM 100Ag/100La at 800°C, can be due to the presence of the silver nanoparticles with SPR and various silver clusters, including Ag_m^{n+} ($m \geq 8$, $n \leq 4$) [48,53]. The absorption bands at 566–570 nm, which are typical for CM 100Ag/10La at 120°C and for all the CM series at 800°C, are, most likely, related to the presence of the silver nanoparticles with SPR, and silver clusters, including Ag_m^{n+} ($m \geq 8$, $n \leq 4$) [11,39,48,53]. The presence of the additional absorption bands in the samples thermally treated at 800°C, at 606 and 664 nm (CM 100Ag), at 670 nm (CM 100Ag/10La), and at 575 and 603 nm (CM 100Ag/100La), can also be related to formation of silver nanoparticles (differently shaped) with SPR and various silver clusters, including Ag_m^{n+} ($m \geq 8$, $n \leq 4$) [11,39,48,53]. Regardless of the composition and the temperature of thermal treatment, all the composite materials (except for CM 100Ag at 800°C) were found the bands with the maxima at 734–748 nm, which can indicate formation of silver clusters, including Ag_m^{n+} ($m \geq 8$, $n \leq 4$), and the silver nanoparticles with SPR [11,38,39 48].

It has established the influence of CM thermal treatment resulting in increase in the intensity of the absorption band for CM at 800°C. Besides, it should be noted that thermal treatment of CM at 800°C (for all the series) results in the optical density spectra demonstrating a large number of the absorption bands related to the presence of silver MCs, silver clusters, including Ag_m^{n+} ($m \geq 8$, $n \leq 4$), and in appearance of the strong wide absorption bands related to the silver nanoparticles with plasmon resonance.

Fig. 6, *a* shows the X-ray diffraction patterns for CMs 100Ag, 100Ag/10La and 100Ag/100La after thermal treatment at 800°C. The X-ray diffraction pattern for CM 100Ag clearly shows multiple peaks at 2θ: 23.36°, 26.62°, 26.99°, 30.90°, 38.14°, 38.55°, 44.30°, 45.26°, 47.69°, 55.66°, 61.15°, 62.90°, 64.37°, 69.78° and 77.40°. The peaks observed at 2θ ($h\,k\,l$): 38.14° (111), 44.30° (200), 64.37° (220) and 77.40° (311) are typical for the cubic modification of the metal Ag^0 (JCPDS № 01-080-4432) [54–56]. Reflections at 2θ ($h\,k\,l$): 26.62° (110), 38.55° (200), 47.69° (211) and 55.66° (220) are assigned to the cubic modification of Ag_2O (JCPDS № 00-043-0997) [57,58]. Peaks at 2θ ($h\,k\,l$): 23.36° (4 0 2), 30.90° (3 1 4), 44.30° (-8 0 8), 45.26° (2 2 6), 47.69° (-5 1 11), 55.66° (1 3 1), 61.15° (1 3 6), 62.90° (1 3 7) are related to crystallization of the monoclinic modification of SiO_2, tridymite (Tridymite-M, JCPDS № 00-018-1170) [59,60]. The peaks at 2θ ($h\,k\,l$) are visible: 26.99° (100), 55.66° (202) and 69.78° (301), which are assigned to the hexagonal modification Quartz low HP (High-Purity Quartz), SiO_2 (JCPDS № 01-083-2470) [61]. CMs 100Ag/10La and 100Ag/100La are characterized by a lesser number of the peaks at 2θ: 38.04°, 44.15°, 64.48°, 77.31° and 21.24°, 29.32°, 38.02°, 44.19°, 48.58°, 64.32°, 77.35°, respectively. The reflections observed for CMs 100Ag/10La and 100Ag/100La at 2θ ($h\,k\,l$) = 38.02° (111), 38.04° (111), 44.15° (200), 44.19° (200), 64.32° (220), 64.48° (220), 77.31° (311) and 77.35° (311) are assigned to the cubic modification of metal Ag (JCPDS № 01-071-4613) [62]. The peaks observed for CM 100Ag/10La and CM 100Ag/100La at 2θ ($h\,k\,l$) = 29.32° (1 0 -1), 38.02° and 38.04° (1 0 -2), 44.15° and 44.19° (1 0 0)

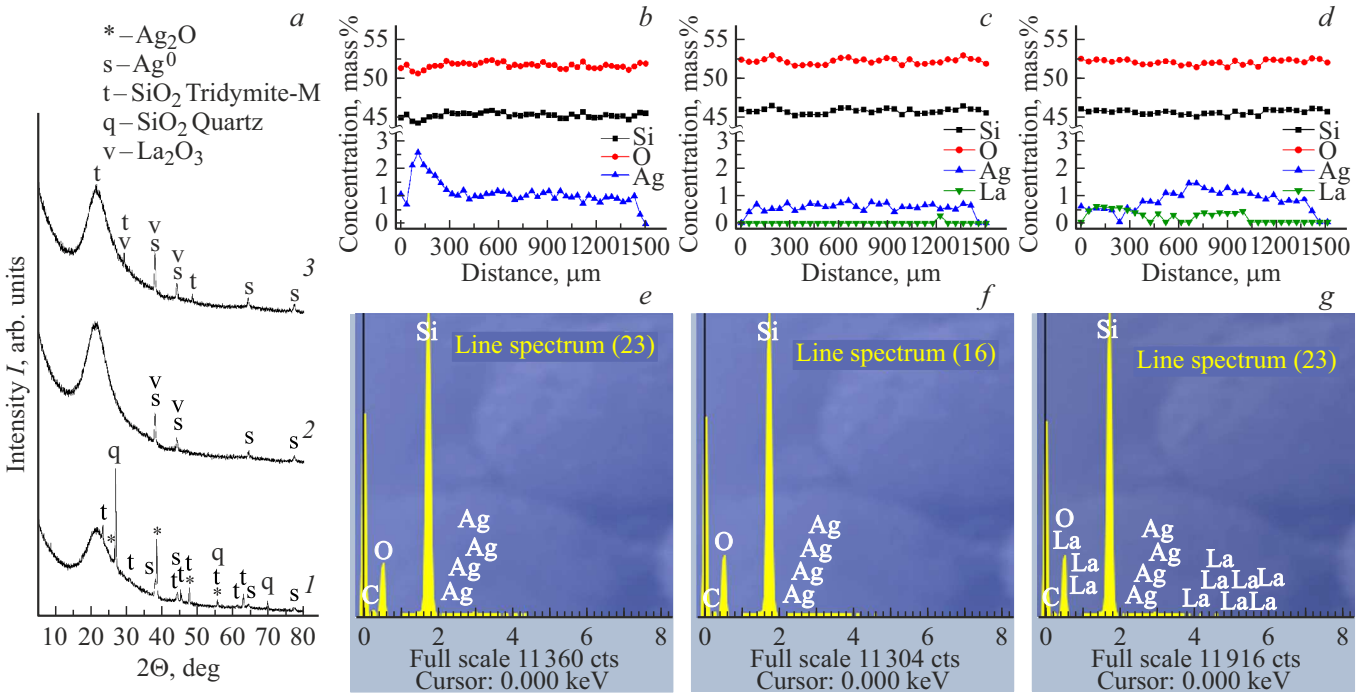

Figure 6. X-ray diffraction patterns for CMs at 800°C depending on the composition (*a*) (*1* — 100Ag, *2* — 100Ag/10La, *3* — 100Ag/100La). EDS data: concentration profiles of the elements along the thickness of the samples (*b*–*d*) and typical spectra of the elemental composition of the central part of the CM samples (*e*–*g*) at 800°C depending on the composition (*b*, *e*) — 100Ag, *c*, *f* — 100Ag/10La, *d*, *g* — 100Ag/100La).

are assigned to the hexagonal modification of La_2O_3 (JCPDS № 00-040-1279) [63]. The weak peaks for CM 100Ag/100La at 2θ ($h\,k\,l$) = 21.24° (-4 0 4), 29.32° (-6 0 4) and 48.58° (-8 0 10) are related to the monoclinic modification Tridymite-M, syn SiO_2 (JCPDS № 00-018-1170) [59,60].

Using the energy-dispersive X-ray spectroscopy, the CMs have been investigated depending on a composition thereof (100Ag, 100Ag/10La and 100Ag/100La) after thermal treatment at 800°C. Fig. 6, *b*–*d* shows the concentration profiles of the elements along the thickness of the CM samples, so does Fig. 6, *e*–*g* typical spectra of the elemental composition of the central part of the CM samples. It should be noted that boron and nitrogen are not detected using the energy-dispersive X-ray spectroscopy, as they are light elements. Distribution of oxygen and silicon is quite uniform along the entire depth of the CM samples. The content of oxygen ans silicon for the CM samples 100Ag is within 50.57–52.31 mas% (the average value: 51.61 ± 0.33 mas%) and 44.23–45.84 mas% (the average value: 45.23 ± 0.30 mas%), for CM 100Ag/10La — 51.52–52.86 mas% (the average value: 52.11 ± 0.33 mas%) and 45.12–46.36 mas% (the average value: 45.69 ± 0.30 mas%), for CM 100Ag/100La — 51.12–52.30 mas% (the average value: 51.81 ± 0.34 mas%) and 44.75–45.87 mas% (the average value: 45.40 ± 0.31 mas%), respectively. The concentration of sodium in all the samples was below a device's sensitivity level (we observe zero values along the entire depth of the samples), while the concentration of lanthanum in CM 100Ag/10La and CM 100Ag/100La was also insufficient (we observed zero values almost along the entire depth of the samples) for determination of the concentration of the element, which should be at least 0.1–0.2 mas%.

Fig. 6, *c*, *d* clearly shows separate concentration „bursts" of the lanthanum distribution for CM 100Ag/10La at 0.27 mas% and for CM 100Ag/100La within 0.25–0.58 mas% (the average value of 0.20 ± 0.15 mas%). Silver is distributed unevenly along the thickness of the samples of CM 100Ag and CM 100Ag/100La, while, on the contrary, silver in CM 100Ag/10La is uniformly enough distributed except for the surface layer of the samples (~ 100 μm).

The content of silver in CM 100Ag changes along the thickness within 0.00–2.60 mas% (the average value: 1.11 ± 0.20 mas%), so does in CM 100Ag/10La within 0.00–0.81 mas% (the average value: 0.55 ± 0.17 mas%), so does in CM 100Ag/100La within 0.00–1.41 mas% (the average value: 0.78 ± 0.17 mas%). The typical spectra of the elemental composition of the central part of the CM samples (Fig. 6, *e*–*g*) were found peaks, corresponding to the main components (the strong peaks — Si, O), the weak and strong peaks of lanthanum, the weak peaks of silver. Similar data for location of the peaks of silver and lanthanum were found in [1,64,65].

Conclusion

The CM samples have been synthesized based on the matrices made of the high-silica porous glasses activated by the silver ions in the presence or without the lanthanum ions, which have been thermally treated in the air atmosphere from 120 to 800°C. Using the X-ray powder diffraction method, it has been established that CMs (at 800°C) had the crystals of the cubic modification of metal Ag^0, the cubic modification of Ag_2O, the hexagonal modification of La_2O_3, the monoclinic modification Tridymite-M and the hexagonal modification Quartz low HP. Using the near IR spectroscopy, CMs have been investigated to demonstrate that CMs activated with the ions of silver and lanthanum showed the additional bands due to the presence of the OH groups, which can coordinate to the several adjacent atoms of lanthanum. Using the optical spectroscopy, it has been confirmed that in various conditions of the synthesis, CMs were characterized by the presence of the absorption bands, which were responsible charge transfer $O^{2-} \rightarrow La^{3+}$ (282, 285, 300 nm) and for the lanthanum nanoparticles (282, 285 nm).

Acknowledgments

The authors would like to thank A.V. Antonov (VSEGEI, Saint-Petersburg) for the CM research using the energy-dispersive X-ray spectroscopy.

The CM crystal structure was investigated using the X-ray powder diffraction method on the equipment belonging to Engineering Center of SPbSTI (TU).

Funding

The work was supported by the Ministry of Sciences and Higher Education of the Russian Federation as part of the IChS RAS state assignment (State registration № AAAA-A19-119022290087-1 and № 1021050501068-5-1.4.3 (FFEM-2022-0004 project)).

Conflict of interest

The authors declare that they have no conflict of interest.

References

[1] G. Abdulkareem-Alsultan, N. Asikin-Mijan, N. Mansir, H.V. Lee, Z. Zainal, A. Islam, Y.H. Taufiq-Yap. J. Analyt. Appl. Pyrolysis, **137**, 171 (2019). DOI: 10.1016/j.jaap.2018.11.023

[2] C.R. Michel, A.H. Martínez-Preciado. Sensors and Actuators B: Chemical, **208**, 355 (2015). DOI: 10.1016/j.snb.2014.11.034

[3] J. Fonseca. Frontiers of Materials Science, **16**, 220607 (2022). DOI: 10.1007/s11706-022-0607-7

[4] M.A.U. Haq, K. Hussain, Z. Aslam, A.R. Umar, M.R. Shan, Sirajuddin, Mujeeb-ur-Rehman, S.T.H. Sherazi, J. Nisar. Microchemical J., **185**, 108289 (2023). DOI: 10.1016/j.microc.2022.108289

[5] H.M.A. Dayem, S.S. Al-Shihry, S.A. Hassan. J. Rare Earths, **37** (5), 500 (2019). DOI: 10.1016/j.jre.2018.09.003

[6] N. Zhao, M.-M. Yao, F. Li, F.-P. Lou. J. Solid-State Chemistry, **184** (10), 2770 (2011). DOI: 10.1016/j.jssc.2011.08.014

[7] Y. Gao, Y. Masuda, K. Koumoto. J. Colloid and Interface Science, **274**, 392 (2004). DOI: 10.1016/j.jcis.2004.02.050

[8] G. Gao, L. Yang, B. Dai, F. Xia, Z. Yang, S. Guo, P. Wang, F. Geng, J. Han, J. Zhu. Surface & Coatings Technology, **365**, 164 (2019). DOI: 10.1016/j.surfcoat.2018.07.001

[9] Q. Mu, Y. Wang. J. Alloys and Compounds, **509** (2), 396 (2011). DOI: 10.1016/j.jallcom.2010.09.041

[10] M.A. Girsova, T.V. Antropova, G.F. Golovina, I.N. Anfimova, L.N. Kurilenko, M.Yu. Arsent'ev. IOP Conference Series: Materials Science and Engineering, **704**, 012004 (2019). DOI: 10.1088/1757-899X/704/1/012004

[11] M.A. Girsova, L.N. Kurilenko, I.N. Anfimova, M.Yu. Arsent'ev, L.F. Dikaya, E.A. Semenova. Russian Chemical Bulletin, **69** (5), 920 (2020). DOI: 10.1007/s11172-020-2849-9.

[12] M.A. Girsova, G.F. Golovina, L.N. Kurilenko, I.N. Anfimova. Glass Physics and Chemistry, **46** (6), 541 (2020). DOI: 10.1134/S1087659620060097.

[13] R. Jbeli, A. Boukhachem, I.B. Jemaa, N. Mahdhi, F. Saadallah, H. Elhouichet, S. Alleg, M. Amlouk, H. Ezzaouïa. Spectrochim. Acta Part A: Molecular and Biomolecular Spectroscopy, **184** (5), 71 (2017). DOI: 10.1016/j.saa.2017.04.072

[14] T. Antropova, M. Girsova, I. Anfimova, I. Drozdova, I. Polyakova, N. Vedishcheva. J. Non-Crystalline Solids, **401**, 139 (2014). DOI: 10.1016/j.jnoncrysol.2014.01.033

[15] M.A. Girsova, G.F. Golovina, L.N. Kurilenko, I.N. Anfimova. Glass Physics and Chemistry, **47** (Suppl. 1), S36 (2021). DOI: 10.1134/S1087659621070051

[16] R.A. Lidin, L.L. Andreeva, V.A. Molochko. *Konstanty neorganichekikh veshchestv: spravochnik* (Drofa, Moskva, 2008), 73, 124 (in Russian).

[17] K. Otto, I.O. Acik, M. Krunks, K. Tönsuaadu, A. Mere. J. Thermal Analysis and Calorimetry, **118**, 1065 (2014). DOI: 10.1007/s10973-014-3814-3

[18] T.V. Antropova. *Fiziko-khimicheskite protsessy cozdaniya poristykh stekol i vysokokremnezemnykh materialov na osnove likviruyushchikh shchelochnoborosilikantnykh sistem*. Diss. dokt. khim. nauk. (Institut khimii silikatov im. I.V. Grebenshchikova RAN, Sankt-Peterburg, 2005), 588 pages (in Russian).

[19] T.V. Antropova, I.A. Drozdova. Optica Applicata, **33** (1), 13 (2003).

[20] T.V. Antropova, A.V. Volkova, D.V. Petrov, S.V. Stolyar, L.E. Ermakova, M.P. Sidorova, E.B. Yakovlev, I.A. Drozdova. Optica Applicata, **35** (4), 717 (2005).

[21] T.V. Antropova, I.A. Drozdova, T.N. Vasilevskaya, A.V. Volkova, L.E. Ermakova, M.P. Sidorova. Glass Physics and Chemistry, **33** (2), 109 (2007). DOI: 10.1134/S1087659607020034.

[22] T.V. Antropova, S.V. Stolyar, I.N. Anfimova, M.A. Girsova. Glass Physics and Chemistry, **47** (4), 329 (2021). DOI: 10.1134/S1087659621040040.

[23] A. Igityan, N. Aghamalyan, S. Petrosyan, I. Gambaryan, G. Badalyan, R. Hovsepyan, Y. Kafadaryan. Appl. Phys. A, **123**, 448 (2017). DOI: 10.1007/s00339-017-1057-4

[24] T.A. Hamdalla, T.A. Hanafy. Optik, **127** (2), 878 (2016). DOI: 10.1016/j.ijleo.2015.10.187

[25] V.A. Nikitin, A.N. Sidorov, A.V. Karyakin. Russian Journal of Physical Chemistry, **30** (1), 117 (1956).
[26] O. Humbach, H. Fabian, U. Grzesik, U. Haken, W. Heitmann. J. Non-Crystalline Solids, **203**, 19 (1996). DOI: 10.1016/0022-3093(96)00329-8
[27] A. Baraldi, R. Capelletti, N. Chiodini, C. Mora, R. Scotti, E. Uccellini, A. Vedda. Nuclear Instruments and Methods in Physics Research A, **486** (1–2), 408 (2002). DOI: 10.1016/S0168-9002(02)00743-X
[28] M.A. Girsova, G.F. Golovina, I.N. Anfimova, L.N. Kurilenko. Glass Physics and Chemistry, **44** (5), 381 (2018). DOI: 10.1134/S1087659618050061.
[29] M.A. Girsova, G.F. Golovina. Glass Physics and Chemistry, **44** (6), 569 (2018). DOI: 10.1134/S1087659618060068.
[30] M.A. Girsova, G.F. Golovina, L.N. Kurilenko, I.N. Anfimova. Glass Physics and Chemistry, **46** (6), 531 (2020). DOI: 10.1134/S1087659620060085.
[31] M.A. Girsova, T.V. Antropova, G.F. Golovina, I.N. Anfimova, L.N. Kurilenko. Opt. Spectrosc., **131** (1), 80 (2023). DOI: 10.21883/EOS.2023.01.55521.4040-22.
[32] J.T. Kloprogge, R.D. Schuiling, Z. Ding, L. Hickey, D. Wharton, R.L. Frost. Vibrational Spectroscopy, **28** (2), 209 (2002). DOI: 10.1016/S0924-2031(01)00139-4
[33] U. Bauer, H. Behrens, M. Fechtelkord, S. Reinsch, J. Deubener. J. Non-Crystalline Solids, **423**–**424**, 58 (2015). DOI: 10.1016/j.jnoncrysol.2015.05.004
[34] R. Balzer, H. Behrens, S. Schuth, T. Waurischk, S. Reinsch, R. Müller, M. Fechtelkord, J. Deubener. J. Non-Crystalline Solids, **519**, 119454 (2019). DOI: 10.1016/j.jnoncrysol.2019.05.030
[35] D.A. Klyukin, V.D. Dubrovin, A.S. Pshenova, S.E. Putilin, T.A. Shakhverdov, A.N. Tsypkin, N.V. Nikonorov, A.I. Sidorov. Optical Engineering, **55** (6), 067101 (2016). DOI: 10.1117/1.OE.55.6.067101
[36] M.V. Stolyarchuk, A.I. Sidorov. Opt. Spectrosc., **125** (3), 305 (2018). DOI: 10.1134/s0030400x18090229.
[37] B.G. Ershov, E.A. Abkhalimov, N.L. Sukhov. High Energy Chemistry, **39** (2), 55 (2005). DOI: 10.1007/s10733-005-00261
[38] M. Mostafavi, M.O. Delcourt, G. Picq. Radiation Physics and Chemistry, **41** (3), 453 (1993). DOI: 10.1016/0969-806x(93)90004-e
[39] B.M. Sergeev, G.B. Sergeev. Colloid J., **69**(5), 639 (2007). DOI: 10.1134/S1061933X07050158.
[40] J.-G. Kang, Y.-Il Kim, D.W. Cho, Y. Sohn. Materials Science in Semiconductor Processing, **40**, 737 (2015). DOI: 10.1016/j.mssp.2015.07.050
[41] R. Dovnar, A. Vasilkov, I. Dovnar, N. Iaskevich. Cardiology in Belarus, **15** (1), 99 (2023). DOI: 10.34883/PI.2023.15.1.008 (in Russian).
[42] S. Lecoultre, A. Rydlo, J. Buttet, C. Félix, S. Gilb, W. Harbich. The J. Chemical Physics, **134**, 184504 (2011). DOI: 10.1063/1.3589357
[43] G.A. Ozin, H. Huber. Inorganic Chemistry, **17** (1), 155 (1978).
[44] S. Fedrigo, W. Harbich, J. Buttet. J. Chem. Phys., **99** (8), 5712 (1993). DOI: 10.1063/1.465920
[45] C. Félix, C. Sieber, W. Harbich, J. Buttet, I. Rabin, W. Schulze, G. Ertl. Chem. Phys. Lett., **313**, 105 (1999).
[46] A.V. Vostokov, A.I. Ignat'ev, N.V. Nikonorov, O.A. Podsvirov, A.I. Sidorov, A.V. Nashchekin, R.V. Sokolov, O.A. Usov, V.A. Tsekhomskii. Technical Physics Letters, **35** (9), 812 (2009). DOI: 10.1134/S1063785009090089.
[47] C.G. Hu, H. Liu, W.T. Dong, Y.Y. Zhang, G. Bao, C.S. Lao, Z.L. Wang. Advanced Materials, **19** (3), 470 (2007). DOI: 10.1002/adma.200601300
[48] A.J. Haes, C.L. Haynes, A.D. McFarland, G.C. Schatz, R.P. Van Duyne, S. Zou. MRS Bulletin, **30**, 368 (2005). DOI: 10.1557/mrs2005.100
[49] M.C. Mathpal, P. Kumar, S. Kumar, A.K. Tripathi, M.K. Singh, J. Prakash, A. Agarwal. RSC Advances, **5** (17), 12555 (2015). DOI: 10.1039/c4ra14061c
[50] A.E. Abbass, H.C. Swart, R.E. Kroon. J. Sol-Gel Science and Technology, **76** (3), 708 (2015). DOI: 10.1007/s10971-015-3825-y
[51] M.V. Shestakov, M. Meledina, S. Turner, V.K. Tikhomirov, N. Verellen, V.D. Rodríguez, J.J. Velázquez, G. Van Tendeloo, V.V. Moshchalkov. J. Appl. Phys., **114** (7), 073102 (2013). DOI: 10.1063/1.4818830
[52] P.A. Obraztsov, A.V. Nashchekin, A.V. Panfilova, P.N. Brunkov, N.V. Nikonorov, A.I. Sidorov. Physics of the Solid State, **55** (6), 1272 (2013). DOI: 10.1134/S1063783413060267.
[53] J. Belloni, M. Mostafavi, H. Remita, J.-L. Marignier, M.-O. Delcourt. New J. Chemistry, **22** (11), 1239 (1998). DOI: 10.1039/a801445k
[54] H.A. Oualid, Y. Essamlali, O. Amadine, K. Daanoun, M. Zahouily. Ceramics International, **43** (16), 13786 (2017). DOI: 10.1016/j.ceramint.2017.07.097
[55] H.A. Oualid, O. Amadine, Y. Essamlali, I.M. Kadmiri, H.El. Arroussi, M. Zahouily. Nanoscale Advances, **1** (8), 3151 (2019). DOI: 10.1039/c9na00075e
[56] C. Tonna, C. Wang, D. Mei, S.V. Lamaka, M.L. Zheludkevich, J. Buhagiar. Bioactive Materials, **7**, 426 (2022). DOI: 10.1016/j.bioactmat.2021.05.48
[57] H. Xu, J. Xie, W. Jia, G. Wu, Y. Cao. J. Colloid and Interface Science, **516**, 511 (2018). DOI: 10.1016/j.jcis.2018.01.071
[58] H. Yang, J. Tian, T. Li, H. Cui. Catalysis Communications, **87**, 82 (2016). DOI: 10.1016/j.catcom.2016.09.013.
[59] V.A. Kukartsev, A.I. Cherepanov, V.V. Kukartsev, V.S. Tynchenko, V.V. Bukhtoyarov, A.M. Popov, R.B. Sergienko, S.V. Tynchenko. Minerals, **12** (2), 233 (2022). DOI: 10.3390/min12020233
[60] E.B. Shadrin, D.A. Kurdyukov, A.V. Ilinskiy, V.G. Golubev. Semiconductors, **43** (1), 102 (2009). DOI: 10.1134/S1063782609010205.
[61] W.S. Geleta, E. Alemayehu, B. Lennartz. Molecules, **27**, 2527 (2022). DOI: 10.3390/molecules27082527
[62] S. Al-Thawadi, A.S.A. Rasool, K. Youssef. J. Bioanalysis & Biomedicine, **9** (6), 299 (2017). DOI: 10.4172/1948-593X.1000197
[63] K. Shah, K. Agheda, M. Ahire, K.V.R. Murthy, B. Chakrabarty. Bull. Mater. Sci., **46**, 186 (2023). DOI: 10.1007/s12034-023-03012-3
[64] A. Igityan, N. Aghamalyan, R. Hovsepyan, S. Petrosyan, G. Badalyan, I. Gambaryan, A. Papikyan, Y. Kafadaryan. Semiconductors, **54** (2), 163 (2020). DOI: 10.1134/S1063782620020104.
[65] K. Wang, Y. Wu, H. Li, M. Li, F. Guan, H. Fan. J. Inorganic Biochemistry, **141**, 36 (2014). DOI: 10.1016/j.jinorgbio.2014.08.009

Translated by M.Shevelev